INORGANIC CHEMISTRY
FRONTIERS

RESEARCH ARTICLE

View Article Online
View Journal | View Issue

Cite this: *Inorg. Chem. Front.*, 2025, **12**, 3073

Ionic radius-dependent self-assembly of lanthanide organic polyhedra: structural diversities and luminescent properties†

Jing Su,[a,b,c] Fan Yin,[a] Xiao-Fang Duan,[a] Jing-Yao Zhou,[a] Li-Peng Zhou,[a] Chong-Bin Tian *[a,b,c] and Qing-Fu Sun *[a,b,c]

The synthesis of nonclassical polyhedra is at the forefront of supramolecular research because of their unique anisotropic interior cavities. However, due to the difficulty in controlling the topology of Ln supramolecular systems, the preparation of nonclassical lanthanide organic polyhedrals (LOPs) remains a challenge. Herein, we explore the ionic radius-dependent self-assembly of LOPs using a rectangular tetra-tropic ligand **L**. Owing to the rectangular geometry of the ligand panels (rather than square), its assembly with lanthanide ions located in the middle of the Ln series afforded an irregular tetragonal antiprismatic Ln_8L_4 (Ln = Sm^{3+}, Eu^{3+}, Tb^{3+}, Dy^{3+} and Ho^{3+}) with two faces unoccupied with **L** ligands. Interestingly, this tetragonal antiprism possessed an oblate internal cavity that binds to four THF molecules in the solid-state structure. With an increase in radius, the larger La^{3+} and Nd^{3+} ions produced Ln_4L_2 with a distinct sandwich square architecture. In contrast, the smaller Er^{3+} and Lu^{3+} ions gave rise to a mixture of both Ln_8L_4 and Ln_6L_3. On adding excess Ln^{3+} ions, a structural transformation from Ln_8L_4 to Ln_6L_3 occurred. Structural comparisons of La_4L_2 and Sm_8L_4 revealed that the differences in architecture within these systems were governed by both the ionic radii of the lanthanides and conformational flexibility of the ligands. Photophysical investigations revealed that the ligand **L** exhibited a sensitizing ability toward Sm^{3+}, Tb^{3+} and Dy^{3+} ions, displaying their characteristic luminescence emission, with a new record-setting luminescent quantum yield of 92.74% observed for Tb_8L_4. This work provides new insights into the effect of lanthanide size on the resulting assemblies and opens new avenues to develop nonclassical LOPs.

Received 24th January 2025,
Accepted 20th February 2025

DOI: 10.1039/d5qi00265f

rsc.li/frontiers-inorganic

Introduction

Over the past two decades, preparation of self-assembled metal organic polyhedra has emerged as one of the most active research areas in supramolecular chemistry owing to their diverse potential applications, which include, but are not limited to, supramolecular catalysis,[1–5] molecular recognition and separation,[6–11] drug delivery[12–15] and guest binding.[16–22] In this context, the advancement of lanthanide organic polyhedra (LOPs) is of particular interest. This interest is driven by the intrinsic optical, catalytic and magnetic properties of Ln ions,[23–27] which can be integrated into the final LOPs by the Ln center. However, research on synthesizing such LOPs remains in its infancy compared to transition coordination assemblies, and only a limited number of such supramolecular architectures have been reported.[28,29] This is primarily caused by the variable coordination numbers, weak coordination abilities, diverse coordination geometries, and poor stereochemical preferences of Ln ions.

Octanuclear LOPs with cubic or tetragonal prismatic architectures can be constructed by combining the C_2 symmetric di-tropic tridentate or C_4 symmetric tetra-tropic tridentate ligands with nine-coordinated Ln centers. They typically form cubic structures that can be represented by the formulas Ln_8L_{12} (L = C_2-symmetric ligands) or Ln_8L_6 (L = C_4-symmetric ligands) based on the geometric matching principle between the ligand and Ln^{3+} ions, which was proposed by Raymond and co-workers.[30] To date, several Ln_8L_{12} or Ln_8L_6 compounds have been successfully developed by our group and other groups.[31–36] Nevertheless, most of the reported Ln_8L_{12} or Ln_8L_6 assemblies exhibit high-symmetry structures with

[a]*State Key Laboratory of Structural Chemistry, Fujian Institute of Research on the Structure of Matter, Chinese Academy of Sciences, Fuzhou 350002, P. R. China. E-mail: tianchongbin@fjirsm.ac.cn, qfsun@fjirsm.ac.cn*
[b]*College of Chemistry and Materials Science, Fujian Normal University, Fuzhou, 350007, China*
[c]*Fujian College, University of Chinese Academy of Sciences, Fuzhou, Fujian, 350002, P. R. China*

†Electronic supplementary information (ESI) available: Detailed synthesis, X-ray crystallographic data, NMR, MS, UV-Vis, FL and other physical measurements. CCDC 2413380–2413382 and 2413524. For ESI and crystallographic data in CIF or other electronic format see DOI: https://doi.org/10.1039/d5qi00265f

regular Archimedean or Platonic geometries. In contrast, non-classical Archimedean or Platonic octanuclear LOPs with missing linkers or faces have been rarely reported[37,38] owing to the challenges associated with controlling the topology of Ln supramolecular systems.

One intriguing aspect of metal organic polyhedra is their dynamic and reversible metal–ligand bonds, which can be utilized to modify their structure by changing factors such as metal ions,[39–42] stoichiometry,[43,44] concentration,[31,45,46] anions,[47,48] pH[49,50] and some others.[51,52] Among these factors, the selection of metal ions is particularly significant in the design of metal organic polyhedra.[39–42] The differences in the radii of metal centers can endow the cages with an extra degree of flexibility through the rearrangement of the coordination chelating unit, resulting in the generation of some new species. Along this line, a gradual change in the effective ionic radius across the lanthanide series, known as "lanthanide contraction", makes Ln^{3+} ions ideal candidates for these studies. For example, Hooley and our team demonstrated that the Ln-selective self-assembly can occur through multivalency and cooperativity, which have potential utilization in Ln separation using a supramolecular approach.[7,53] Recently, our group developed a post-synthetic transmetalation self-assembly strategy for creating near infrared emitting Yb_8L_6 cube, which cannot be achieved using a direct synthesis method.[34] A deeper understanding of the specific role of Ln^{3+} ions in the self-assembly process can facilitate the rational design of LOPs and promote the discovery of novel Ln supramolecular architectures that go beyond traditional approaches. Consequently, more examples of ionic radius-dependent self-assembly of LOPs are required.

Based on the considerations mentioned above, we report the design and synthesis of a rectangular tetra-tropic tridentate ligand, **L**, derived from 2,6-di[pyrazol-1-yl]pyridine (bpp) chelating moieties. Its self-assembly with lanthanide ions leads to a series of distinct $Ln_{2n}L_n$ (n = 2, 3 and 4) assemblies with the unsaturated metal sites: sandwich square Ln_4L_2, the triangular prism Ln_6L_3, and the unique twisted tetrahedron prism Ln_8L_4. These assemblies were characterized by a combination of NMR, mass spectrometry, and single-crystal X-ray analysis. We found that the formation of these assemblies depends on the ionic radii of the Ln series as well as the varying conformation of the ligands. Additionally, the photophysical properties of Sm_8L_4, Tb_8L_4 and Dy_8L_4 were investigated.

Results and discussion

Ligand design, synthesis and assembly with lanthanides

The tetra-tropic ligands are commonly employed to fabricate octanuclear metal organic polyhedra. However, the square geometry of these ligand panels results in a regular cubic configuration of octanuclear assemblies.[34,54–59] To create octanuclear assemblies using the nonclassical Archimedean or Platonic solids, designing ligands with rectangular panels may be a promising strategy, as recently demonstrated by Nitschke *et al.* in their subcomponent self-assembled transition-based metal–organic architectures.[60,61] In addition, tetra-tropic ligands contain very complex conformations, which can enhance the structural complexity and diversity after coordination with metal ions. The 2,6-di[pyrazol-1-yl]pyridine (bpp) and its derivatives are widely used tridentate coordination units in constructing transition metal complexes.[62,63] However, this motif has been less explored in preparing rare earth coordination compounds.[64,65] Consequently, we opted to introduce bpp tridentate chelating units into the tetra-tropic ligand, and its assembly with Ln^{3+} ions generally afforded octanuclear LOPs. The tetra-topic tridentate ligand **L** was synthesized by Suzuki coupling (the experimental details are shown in the Experimental section of the ESI†) and was characterized by NMR.

Synthesis and characterization of La_4L_2

When 2.0 equiv. of ligand **L** was treated with 4.0 equiv. of La $(OTf)_3$ in acetonitrile at 70 °C for 30 min, the turbid suspension of the ligand gradually turned into a homogeneous clear solution. The ^{1}H NMR spectrum clearly indicates the generation of La_4L_2 assembly. Compared with the highly symmetric free **L**, the ^{1}H NMR spectrum of La_4L_2 showed 2-fold desymmetrization of the **L** (Fig. 1B and C), in agreement with the D_2 point symmetry of a sandwich square. The DOSY spectrum dis-

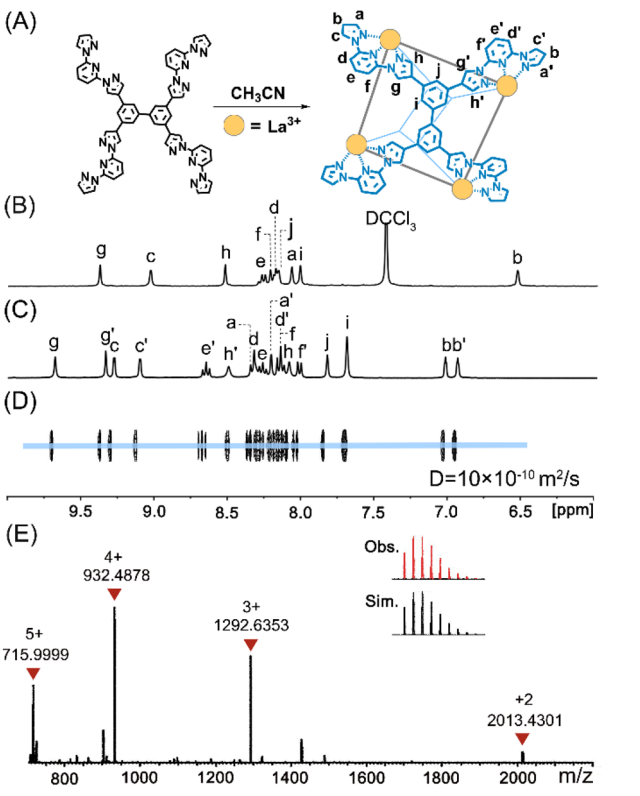

Fig. 1 (A) Self-assembly of L with La(OTf)$_3$. ^{1}H NMR spectra (400 MHz, 298 K) of L in $CDCl_3$ (B) and La_4L_2 in CD_3CN (C). (D) DOSY spectra of La_4L_2. (E) ESI-TOF-MS of La_4L_2 with the inset showing the observed and simulated isotopic patterns of the +4 peak.

plays a single diffusion band with a diffusion coefficient of 10 × 10^{-10} m^2 s^{-1}, corresponding to a hydrodynamic radius of 12.72 Å for La_4L_2 calculated using the Stokes–Einstein equation (Fig. 1D). As shown in Fig. 1E, high-resolution ESI-TOF-MS clearly suggests the presence of sandwich square assembly with a molecular formula of $La_4(L)_2(OTf)_{12}$. A set of prominent peaks was assigned according to the consecutive loss of OTf^- counter ions. For example, peaks with m/z = 715.9999, 932.4878, 1292.6353 and 2013.4301 correspond to $[La_4(L)_2(OTf)_7]^{5+}$, $[La_4(L)_2(OTf)_8]^{4+}$, $[La_4(L)_2(OTf)_9]^{3+}$ and $[La_4(L)_2(OTf)_{10}]^{2+}$, respectively. Moreover, the isotopic pattern of each assignment was in line with the simulated one (Fig. 1E, inset).

Synthesis and characterization of Sm_8L_4

Previous studies have demonstrated that the generation of lanthanide architectures is sensitive to the radius of lanthanide ions.[34,40,53,66–69] Consequently, we hypothesize that using lanthanide ions bearing a smaller radius than La^{3+} ions may lead to the development of a different architecture during the self-assembly process. To our delight, when $Sm(OTf)_3$ was employed as the metal source at the same 2 : 1 metal-to-ligand ratio as La_4L_2, a noticeably different ^1H NMR spectrum was observed, suggesting the formation of a new species. Based on the NMR, ESI-MS, and single-crystal X-ray diffraction data (*vide infra*), the newly formed species is a tetragonal antiprismatic Sm_8L_4 LOP. Analysis of ^1H NMR spectroscopy uncovered a different molecular symmetry compared to La_4L_2. Unlike the two sets of signals for the ligand arms found in La_4L_2, we detected four sets of ligand arm signals after substituting La $(OTf)_3$ with $Sm(OTf)_3$ (Fig. 2B). The proton signals are completely assigned based on ^1H–^1H COSY and NOE 2D spectra (Fig. S14 and S15†). Because the four sets of proton signals exhibit equal intensity on the Sm_8L_4 cage, we conclude that there is only one magnetically distinct ligand, which is in agreement with its S_4 symmetry observed on the solid-state structure (*vide infra*). Evidence for the exclusive formation of a sole species in solution was offered by ^1H diffusion ordered spectroscopy (DOSY), where all signals were located in a single band (Fig. 2C), from which the kinetic diameter of 30.03 Å could be estimated. To verify the stoichiometry of the Sm^{3+} assembly, the ESI-MS spectrum was recorded using acetonitrile as the solvent. The observed peaks at m/z = 822.7847, 944.3536, 1100.4248, 1308.6549, 1600.1769 and 2037.4610 belong to the fragments $[Sm_8(L)_4(OTf)_{15}]^{9+}$, $[Sm_8(L)_4(OTf)_{16}]^{8+}$, $[Sm_8(L)_4(OTf)_{17}]^{7+}$, $[Sm_8(L)_4(OTf)_{18}]^{6+}$, $[Sm_8(L)_4(OTf)_{19}]^{5+}$ and $[Sm_8(L)_4(OTf)_{20}]^{4+}$, respectively. The ESI-MS result certificates a tetragonal prism composition of Sm_8L_4 assembly.

Synthesis and characterization of Lu_6L_3

With the above fascinating finding, we are curious to know whether a new assembly will be formed when using the even smaller Lu^{3+} ion. By replacing the metal source of Sm^{3+} with Lu^{3+}, we observed a distinct ^1H NMR pattern that showed more complicated signals compared with Sm_8L_4 species (Fig. S21†). It was impossible to make a detailed proton assignment because of obvious line broadening and overlapping signals. However, the ESI-MS spectrum indicated the formation of mixed Lu_6L_3 and Lu_8L_4 (Fig. S42†).

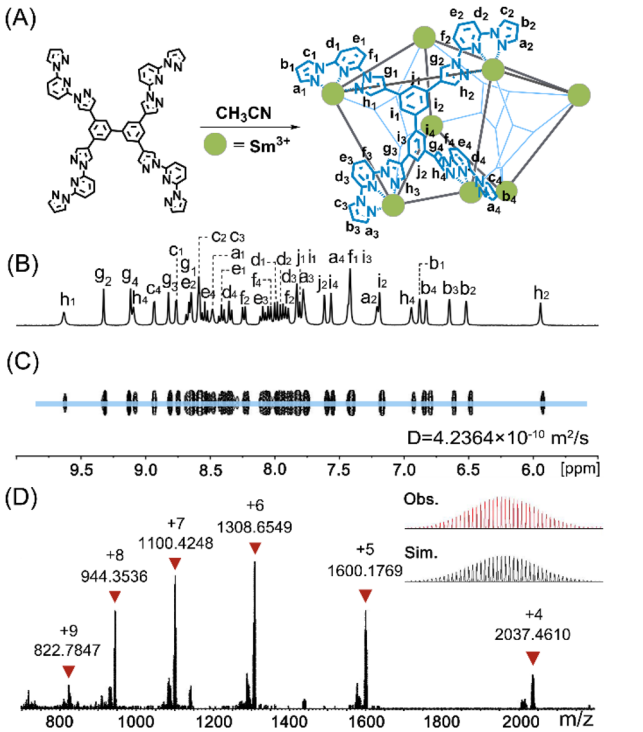

Fig. 2 (A) Self-assembly of L with $Sm(OTf)_3$. (B) ^1H NMR spectra (400 MHz, 298 K) of Sm_8L_4 in CD_3CN. (C) DOSY spectra of Sm_8L_4. (D) ESI-TOF-MS of Sm_8L_4 with the inset showing the observed and simulated isotopic patterns of the +6 peak.

It is known that an excess of metal can trigger an initial assembly transformation into a new species.[68] Inspired by this, we explored the effect of metal excess on the structure. The ^1H NMR titration experiment indicates that the broadening and overlapping signals evolve into a set of well-resolved peaks once the metal-to-ligand ratio reaches 4 : 1 (Fig. S22†), which consists of ten different signals. This simplified ^1H NMR spectrum was also observed by directly assembling the Lu^{3+} ion with L in a metal-to-ligand ratio of 4 : 1. The ESI-MS spectrum of the above solution demonstrates the presence of the hexanuclear complex with chemical formula Lu_6L_3 (Fig. 3A), where the three tetra-topic tridentate ligand L may cover the rectangular faces of Lu_6L_3, and gives a trigonal prism structure (Scheme 1).

Crystal structural analysis of La_4L_2 and Sm_8L_4

The slow diffusion of diethyl ether into the acetonitrile of La_4L_2 for one week led to high-quality single crystals suitable for X-ray structural analysis. Single crystal X-ray diffraction analysis reveals that La_4L_2 crystallizes in the monoclinic $P2_1/n$ space group with a sandwich square structure (Fig. 4A). The asymmetric unit of La_4L_2 consists of one complete La_4L_2 molecule (Fig. S50†), where all four La^{3+} ions are ligated by ten donor atoms and adopt a bicapped square antiprism coordi-

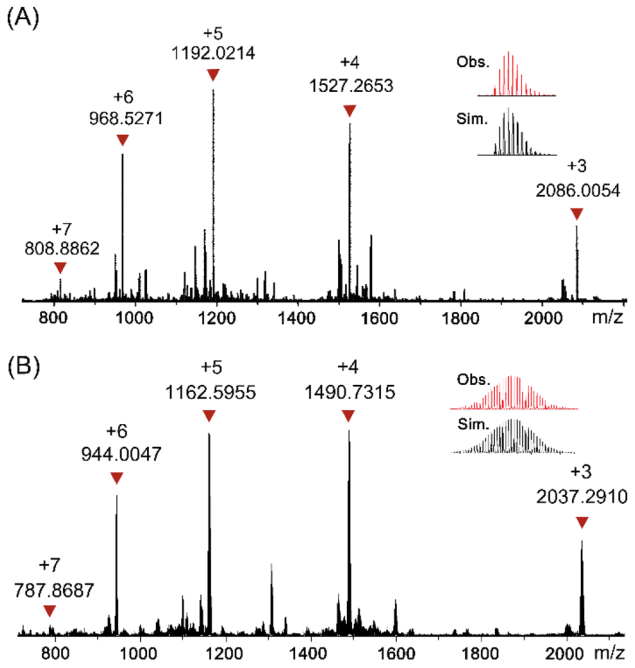

Fig. 3 ESI-MS of Lu_6L_3 (A) and Sm_6L_3 (B) complexes with the insets showing the observed and simulated isotopic patterns of the +5 peak.

nation geometry (Fig. S51 and Table S3†). The dihedral angles between metal-chelating planes around the La^{3+} node are 44.67, 46.02, 46.20 and 45.74° for La1, La2, La3 and La4, respectively (Fig. S52†). Owing to one whole La_4L_2 molecule being observed in the asymmetric unit, its point symmetry in the solid-state structure is C_1 rather than the solution state point symmetry D_2. This behavior should be caused by the different coordinated solvents and different numbers of coordinated OTf^- anions at the La centers, which reduced the symmetry of La_4L_2 in the solid state. Thus, if we remove the coordination solvents and coordinated OTf^- anions, the point symmetry of La_4L_2 can be regarded as D_2 with slight deviations from perfect geometry, which is consistent with the findings from ^1H NMR (*vide supra*). The four La^{3+} ions form a twisted square, with La–La distances of 11.56, 12.55, 11.44 and 12.42 Å (Fig. 4B). In La_4L_2, the two ligands bearing conformation mode A (Fig. 4B and Table S6†) are located above and below the La_4 square, resulting in the metal centers with the same Δ or Λ configuration (Fig. S53†). The distances between the two corresponding phenyl rings belonging to the panels of two ligands, which exhibited a "face-to-face" arrangement mode, were measured to be 3.99 Å and 4.02 Å (Fig. 4C, top). These values indicate the presence of an intermolecular π–π stacking interaction between the two ligands. Furthermore, the average torsion angle between the phenyl ring of the ligand's panel in La_4L_2 is 27.60° (Fig. 4B).

The definitive confirmation of the structure for Sm_8L_4 assembly was provided by a single-crystal diffraction analysis. Crystallographic analysis shows that Sm_8L_4 crystalizes in a tetragonal space group, with one quarter of the cage molecule present in the asymmetric unit (Fig. S54†), featuring a twisted tetragonal antiprismatic structure. The asymmetric unit of Sm_8L_4 consists of two crystallographic independent Sm^{3+} ions,

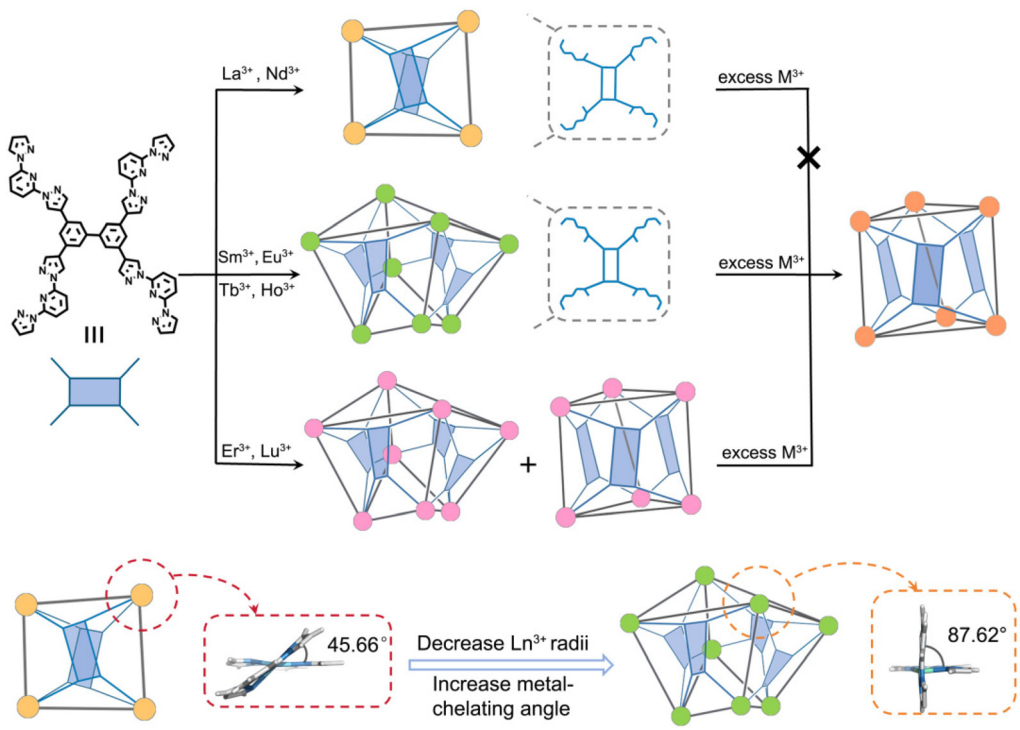

Scheme 1 Ionic radius-dependent self-assembly of LOPs based on rectangular tetra-tropic ligands.

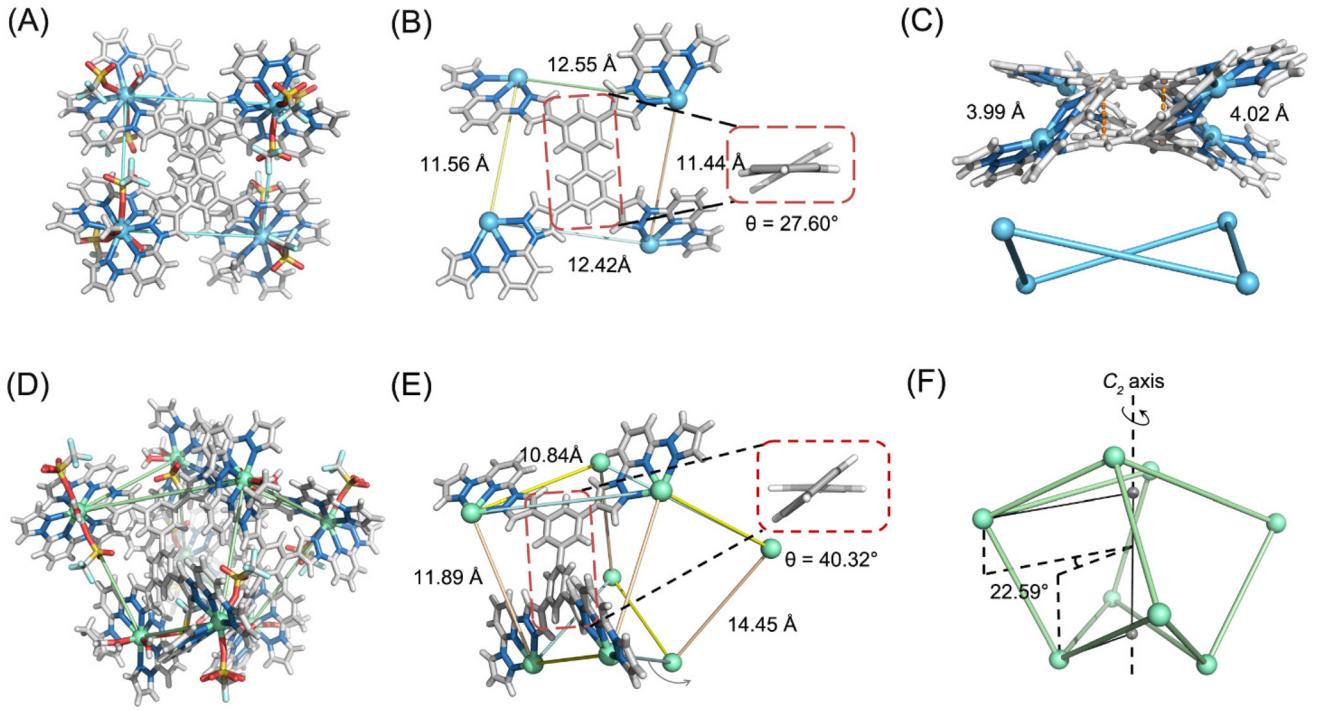

Fig. 4 (A) X-ray single-crystal structure of La_4L_2. (B) Ligand conformation with the La–La distances and average torsion angle between phenyl rings in La_4L_2. (C) π–π stacking interaction between the panels of two ligands. (D) X-ray single-crystal structure of Sm_8L_4. (E) Ligand conformation with the Sm–Sm distances and average torsion angle between phenyl rings in Sm_8L_4. (F) Twist angle of Sm_8L_4, which is defined as the dihedral angle between Sm^{3+} (top face)···centroid (top face)···centroid (bottom face) face and centroid (top face)···centroid (bottom face)···Sm^{3+} (bottom face) face.

both with a coordination number of nine: the Sm1 atom has a tricapped trigonal prism geometry, while the Sm2 atom has a capped square antiprism geometry (Fig. S55 and Table S4†). For Sm1 and Sm2, the dihedral angles between the metal-chelating planes around the Sm^{3+} center are 86.47 and 88.77°, respectively (Fig. S56†). Research into the molecular structure of Sm_8L_4 shows that each ligand bridged four Sm^{3+} ions located on the side face of the twisted tetragonal antiprism. The top and bottom faces of tetragonal antiprism are empty. Moreover, the torsion angle between the phenyl ring of the ligand's panel in Sm_8L_4 is 40.32° (Fig. 4E), leading to the four Sm^{3+} centers on the side face of the tetragonal antiprism not being in the same plane. This result generates the formation of a distorted square on the side face of the tetragonal antiprism. Four such distorted squares together form the highly twisted tetragonal antiprism. The edge length of the tetragonal antiprismatic Sm_8L_4 is 11.89 Å, and the side lengths of the up and bottom distorted squares in the tetragonal antiprismatic Sm_8L_4 are 10.84 Å and 14.45 Å, respectively (Fig. 4E). As shown in Fig. S57,† each tetragonal antiprismatic Sm_8L_4 cage consists of a 1 : 1 radio of Δ-Sm^{3+} and Λ-Sm^{3+} metal vertices, where each Sm^{3+} center is surrounded by the nearest neighbors of the opposite chiral configuration. On each face of the tetragonal antiprism, the Δ-Sm^{3+} and Λ-Sm^{3+} centers are arranged alternately. Such a distribution of metal chiral within Sm_8L_4 gives rise to an overall achiral S_4 molecular symmetry, in which the C_2 rotation axis runs through the centers of the up and bottom faces of tetragonal antiprism (Fig. 4F). The twist angle, defined as the dihedral angle between the face constructed by the top face Sm^{3+}, centroids of the top and bottom faces, is measured to be 22.59° (Fig. 4F). The tetragonal antiprism provides an oblate internal cavity (Fig. S60†), which is different from the pseudospherical or prolate cavities formed by the tetragonal prism.[60,61,70,71] This cavity feature makes the cage suitable for binding small planar guest molecules. To our delight, we found in the crystal structure that four THF molecules occupy the oblate cavity of Sm_8L_4 (Fig. S61†). ^{1}H NMR titration experiment indicates a fast-exchange binding dynamic mode, and the apparent association constants (K_a) for THF are determined to be 127 M^{-1} by applying the Hill function (Fig. S63 and S64†). After removing the THF molecules, the cavity volume of Sm_8L_4 was calculated to be 594.52 $Å^3$ using the MoloVol program.[72]

Extensive attempts to crystallize the Lu_6L_3 were unsuccessful. This failure may be attributed to the presence of excess Lu^{3+} ions in the solution, which could disrupt the crystallization process by promoting the formation of amorphous or poorly ordered competing phases rather than desired Lu_6L_3 single crystals.

To gain insight into the structural changes related to lanthanides, we conducted detailed structural analyses of the two assemblies. Our analysis indicates that both the central lanthanide ions and the conformation of the ligands play a crucial role in the selective formation of the resulting assem-

blies. First, the La^{3+} and Sm^{3+} ions, which have different radii and exhibit different coordination numbers, give rise to the assemblies with different nuclearities. For example, the La^{3+} ion, the largest along the lanthanide series, has a coordination number of ten in La_4L_2. This results in a small average dihedral angle between the metal-chelating planes around the La^{3+} node (Avg: 45.66°), promoting the formation of a sandwich square structure. In contrast, the smaller Sm^{3+} ion has a coordination number of nine in Sm_8L_4. This reduction in the coordination number allows for enough space to increase the dihedral angle between the metal-chelating planes surrounding the Sm^{3+} center, which is essential for the formation of higher nuclearity assemblies. Consequently, a larger average dihedral angle was obtained around the Sm^{3+} node in Sm_8L_4 (Avg: 87.62°), leading to the generation of higher nuclearity Sm_8L_4. Second, the ligand **L** in La_4L_2 and Sm_8L_4 displays different conformations: mode A for La_4L_2 and mode D for Sm_8L_4 (Fig. 4B, E and Table S6†). Third, the average torsion angle between the phenyl ring of the ligand's panel in La_4L_2 and Sm_8L_4 is different: 27.60° in La_4L_2 and 40.32° in Sm_8L_4. Because the metal nodes in La_4L_2 and Sm_8L_4 each contain the same two coordinated bpy moieties, it can be assumed that the main reason for such structural change stems from the decreased lanthanide radius and varied ligand conformation.

Effect of Ln ions on supramolecular architecture

After characterizing the assemblies of La_4L_2, Sm_8L_4 and Lu_6L_3, we determine whether these assemblies were exclusively formed by their corresponding La^{3+}, Sm^{3+} and Lu^{3+} ions, or if they could also be created with alternative lanthanide ions. Specifically, we wanted to investigate whether the structure is affected by ionic radii. To explore this, we conducted further studies using other selected lanthanides (Nd^{3+}, Eu^{3+}, Tb^{3+}, Dy^{3+}, Ho^{3+} and Er^{3+}), which span the Ln series and offer a range of ionic radii. The experiments were carried out using 2 : 1 ratios of lanthanide triflates (Ln = Nd^{3+}, Eu^{3+} and Er^{3+}) and **L** in acetonitrile. For the Nd^{3+} ion, the mass spectrum analysis supported the formation of the Nd_4L_2 complex (Fig. S28†), similar to the results obtained with the La^{3+} ion. However, when the Nd^{3+} ion was replaced with Eu^{3+} ions, the mass spectrum data revealed the production of octanuclear Eu_8L_4 complexes (Fig. S32†), similar to those observed with Sm^{3+} ions. In contrast, the use of the Er^{3+} ion resulted in a mixture of self-assembled species, including Er_8L_4 and Er_6L_3 supramolecular architectures, as evidenced by its mass spectrum (Fig. S40†). Clearly, the structures of assemblies are influenced by the tiny difference in ionic radii across the Ln series, which is consistent with the previous reports.[34,40,53,66–69] The larger lanthanide cations, such as La^{3+} and Nd^{3+}, can form sandwich square structure Ln_4L_2, while the lanthanides positioned in the middle of the series, such as Sm^{3+}, Eu^{3+}, Tb^{3+}, Dy^{3+} and Ho^{3+} (Fig. S30–S39†), can produce tetragonal antiprism Ln_8L_4. In contrast, the smaller lanthanide ions (Ln = Er^{3+} and Lu^{3+}) yield a mixture of both Ln_8L_4 and Ln_6L_3 (Fig. S40–S43†). It is important to highlight that our observations differ from previous reports, which suggested that structural alternation was only caused by ionic radii without observing changes in ligand conformation.[34,40,66–69] In our case, however, the variation in the conformation of ligands was distinctly observed (*vide supra*).

Inspired by the structural transformation from Lu_8L_4 to Lu_6L_3, we subsequently explore whether other lanthanide ions exhibit similar structural changes in the presence of excess Ln^{3+} ions. For La^{3+}, no changes were detected in the ^1H NMR spectrum after adding excess La^{3+} ions into the solution of La_4L_2 (Fig. S23†), indicating that excess La^{3+} ions do not trigger structural conversion. However, for Sm^{3+} ion, the NMR titration experiment of excess Sm^{3+} ions showed the emergence of new NMR peaks when the metal-to-ligand ratio reached 2.8 : 1. At a ratio of 4 : 1, a set of high-symmetry ^1H NMR signals was achieved (Fig. S24†). This high symmetry NMR spectrum is distinctly different from that of Sm_8L_4 but similar to that of Lu_6L_3. This observation may suggest that the excess Sm^{3+} ions can induce the structural transformation from Sm_8L_4 to Sm_6L_3, as the result obtained with Lu^{3+}. The measurement of the mass spectrum demonstrates that the molecular formula of the predominant product after structural transformation was Sm_6L_3 (Fig. 3B). The observations presented above together with the result of the Lu^{3+} ion (*vide supra*) show that excess La^{3+} ions with larger radii are unable to drive structural transformation, while smaller Ln^{3+} ions, such as Sm^{3+} and Lu^{3+} ions, can facilitate such changes. This finding seems to go against traditional knowledge, that is, the smaller the radius of the lanthanide ions, the more stable the resulting complexes and the less likely to suffer structural transformations. Given that the ligand **L** adopts different conformations (mode A in La_4L_2 and Mode D in Sm_8L_4, Table S6†) and exhibits varying torsion angles between panel phenyl rings of the ligand's panel (Fig. 4B and E, 27.60° in La_4L_2 and 40.32° in Sm_8L_4) in the crystal structure of La_4L_2 and Sm_8L_4, we infer that these differences may account for why La_4L_2 is stable and does not undergo structural transformation, while Sm_8L_4 is more labile and capable of such transformation.

Photophysical properties

The UV-vis absorption and luminescence spectra of **L** and Ln_8L_4 (Ln = Sm^{3+}, Tb^{3+}, and Dy^{3+}) were measured in a solution at room temperature. Luminescence analysis data show that the ligand **L** can sensitize Sm^{3+}, Tb^{3+} and Dy^{3+} ions (Fig. 5). Upon the excitation wavelength of 345 nm, the complex Tb_8L_4 exhibits characteristic line-like emission peaks at 487 nm, 543 nm, 585 nm, and 620 nm, which correspond to $^5D_4 \rightarrow {}^6F_J$ (J = 6–3) energy level transition of Tb^{3+} (Fig. 5, top). The quantum yield of Tb_8L_4 in acetonitrile solution is up to 92.74% (Fig. S68†), which is higher than our previously reported tetrahedral Tb^{3+} cage with a record quantum yield of 82% in multinuclear LOPs.[73] Hence, Tb_8L_4 represents a new record-setting quantum yield in multinuclear LOPs. The above results indicate that the ligand **L** has excellent sensitization efficiency towards Tb^{3+}. In contrast, the ligand **L** exhibits relatively poor sensitization ability on Sm^{3+} and Dy^{3+} ions because the quantum yield for Sm_8L_4 and Dy_8L_4 is determined to be

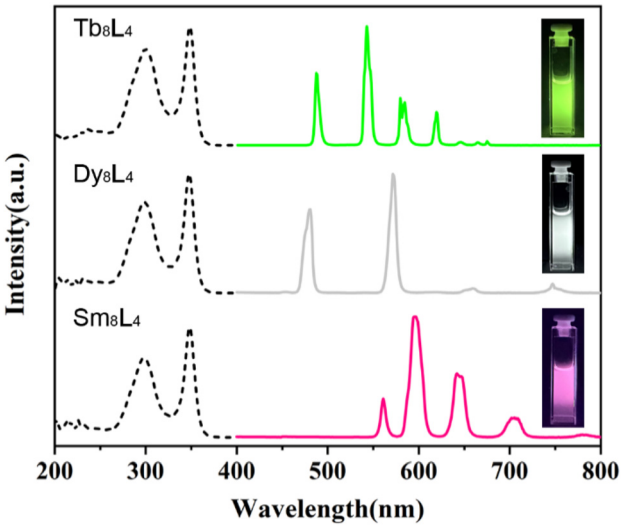

Fig. 5 Excitation (black-dashed lines) and emission (solid color lines) spectra of Tb_8L_4, Dy_8L_4, and Sm_8L_4 in the visible region ($c = 1 \times 10^{-5}$ M, CH_3CN). Insets show the emission under a 365 nm UV light.

0.88% and 2.79% (Table S7†), respectively, which are lower than that of $Tb_8\mathbf{L}_4$. Interestingly, $Dy_8\mathbf{L}_4$ shows single-component white-light emission when excited at 365 nm by UV light (Fig. 5, inset). Because the ligand **L** emits blue light (351 nm, Fig. S72†) and the Dy^{3+} ions mainly exhibit yellow light (572 nm, Fig. S72†), the single-component white-light emission of $Dy_8\mathbf{L}_4$ can be ascribed to the combination of **L**-centered emission and Dy^{3+}-centered emission. To elucidate the different sensitization abilities of ligand **L** to lanthanide ions, we measured the phosphorescence spectrum of the $Gd_8\mathbf{L}_4$ complex at low temperatures (Fig. S75†). The triplet energy level of the ligand was calculated to be 22 523 cm^{-1}, which is closer to the excitation energy level of Tb^{3+} (E = 20 500 cm^{-1}), meaning that ligand **L** exerts a favorable sensitization effect on Tb^{3+}.

Conclusions

In summary, we reported the synthesis and characterization of a series of lanthanide $Ln_{2n}\mathbf{L}_n$ (n = 2, 3, 4) assemblies with tetranuclear sandwich square, hexanuclear triangular prism and octanuclear tetragonal antiprism structures. The larger La^{3+} and Nd^{3+} ions favor the formation of sandwich square structure $Ln_4\mathbf{L}_2$, while with a decrease in radius, the smaller Sm^{3+} and Eu^{3+} give rise to a different structure: the twisted tetragonal prism, $Ln_8\mathbf{L}_4$. Meanwhile, even smaller Er^{3+} and Lu^{3+} ions lose the ability to form exclusively a single species, resulting instead in a mixture of the tetragonal prism, $Ln_8\mathbf{L}_4$, and the trigonal prism, $Ln_6\mathbf{L}_3$. Interestingly, the excess Ln^{3+} ions (Ln = Sm^{3+} and Lu^{3+}) can trigger the structural transformation from $Ln_8\mathbf{L}_4$ to $Ln_6\mathbf{L}_3$. The luminescence investigations revealed that the tetra-topic tridentate ligand based on 2,6-di[pyrazol-1-yl]pyridine can sensitize the luminescence emissions of lanthanide ions simultaneously (Sm^{3+}, Tb^{3+} and Dy^{3+}). Moreover, a record high luminescence quantum yield (Φ = 92.74%) was achieved for $Tb_8\mathbf{L}_4$ assembly. This work demonstrates that the ionic radii of lanthanide affect the resulting supramolecular architectures and that multidentate ligands with rectangular panels are excellent candidates for creating nonclassical Archimedean or Platonic lanthanide solids. Synthesizing additional rectangular multidentate ligands is currently being undertaken to further develop nonclassical LOPs.

Author contributions

Q. F. S. and C. B. T. designed and supervised the project; J. S. completed the synthesis and performed the experiments; F. Y. solved all the crystal structures; X. F. D. and J. Y. Z. analyzed the experiment data; L. P. Z. contributed the mass experiments. S. J., C. B. T. and Q. F. S. wrote the manuscript; all the authors discussed the results and commented on the manuscript.

Data availability

The data supporting this article have been included as part of the ESI.†

Conflicts of interest

There are no conflicts to declare.

Acknowledgements

This work was supported by the National Natural Science Foundation of China (No. 22171264), the Science Foundation of the Fujian Province (No. 2022J01507), and the Self-deployment Project Research Program of Haixi Institutes, Chinese Academy of Sciences (CXZX-2022-GH01).

References

1 M. Yoshizawa, M. Tamura and M. Fujita, Diels-alder in aqueous molecular hosts: Unusual regioselectivity and efficient catalysis, *Science*, 2006, **312**, 251–254.
2 Q.-Q. Wang, S. Gonell, S. H. A. M. Leenders, M. Duerr, I. Ivanovic-Burmazovic and J. N. H. Reek, Self-assembled nanospheres with multiple endohedral binding sites pre-organize catalysts and substrates for highly efficient reactions, *Nat. Chem.*, 2016, **8**, 225–230.
3 H. Takezawa, K. Shitozawa and M. Fujita, Enhanced reactivity of twisted amides inside a molecular cage, *Nat. Chem.*, 2020, **12**, 574–578.

4 M. Morimoto, S. M. Bierschenk, K. T. Xia, R. G. Bergman, K. N. Raymond and F. D. Toste, Advances in supramolecular host-mediated reactivity, *Nat. Catal.*, 2020, **3**, 969–984.
5 Y. Hao, Y.-L. Lu, Z. Jiao and C.-Y. Su, Photocatalysis Meets Confinement: An Emerging Opportunity for Photoinduced Organic Transformations, *Angew. Chem., Int. Ed.*, 2024, **63**, e202317808.
6 X.-Q. Guo, P. Yu, L.-P. Zhou, S.-J. Hu, X.-F. Duan, L.-X. Cai, L. Bao, X. Lu and Q.-F. Sun, Low-symmetry coordination cages enable recognition specificity and selective enrichment of higher fullerene isomers, *Nat. Synth.*, 2025, DOI: 10.1038/s44160-024-00697-0.
7 X.-Z. Li, L.-P. Zhou, L.-L. Yan, Y.-M. Dong, Z.-L. Bai, X.-Q. Sun, D. Juan, W. Shuao, J.-C. Bunzli and Q.-F. Sun, A supramolecular lanthanide separation approach based on multivalent cooperative enhancement of metal ion selectivity, *Nat. Commun.*, 2018, **9**, 547.
8 D. Zhang, T. K. Ronson, Y.-Q. Zou and J. R. Nitschke, Metal-organic cages for molecular separations, *Nat. Rev. Chem.*, 2021, **5**, 168–182.
9 L. J. Wang, S. Bai and Y.-F. Han, Water-Soluble Self-Assembled Cage with Triangular Metal-Metal-Bonded Units Enabling the Sequential Selective Separation of Alkanes and Isomeric Molecules, *J. Am. Chem. Soc.*, 2022, **144**, 16191–16198.
10 P.-F. Cui, X.-R. Liu, Y.-J. Lin, Z.-H. Li and G.-X. Jin, Highly Selective Separation of Benzene and Cyclohexane in a Spatially Confined Carborane Metallacage, *J. Am. Chem. Soc.*, 2022, **144**, 6558–6565.
11 Z. Lu, T. K. K. Ronson, A. W. W. Heard, S. Feldmann, N. Vanthuyne, A. Martinez and J. R. R. Nitschke, Enantioselective fullerene functionalization through stereochemical information transfer from a self-assembled cage, *Nat. Chem.*, 2023, **15**, 405–412.
12 Y.-R. Zheng, K. Suntharalingam, T. C. Johnstone and S. J. Lippard, Encapsulation of Pt(IV) prodrugs within a Pt(II) cage for drug delivery, *Chem. Sci.*, 2015, **6**, 1189–1193.
13 J. E. M. Lewis, E. L. Gavey, S. A. Cameron and J. D. Crowley, Stimuli-responsive Pd_2L_4 metallosupramolecular cages: towards targeted cisplatin drug delivery, *Chem. Sci.*, 2012, **3**, 778–784.
14 Z.-E. Zhang, Y.-F. Zhang, Y.-Z. Zhang, H.-L. Li, L.-Y. Sun, L.-J. Wang and Y.-F. Han, Construction and Hierarchical Self-Assembly of Multifunctional Coordination Cages with Triangular Metal-Metal-Bonded Units, *J. Am. Chem. Soc.*, 2023, **145**, 7446–7453.
15 Y.-H. Huang, Y.-L. Lu, Z.-M. Cao, X.-D. Zhang, C.-H. Liu, H.-S. Xu and C.-Y. Su, Multipocket Cage Enables the Binding of High-Order Bulky and Drug Guests Uncovered by MS Methodology, *J. Am. Chem. Soc.*, 2024, **146**, 21677–21688.
16 P. Mal, B. Breiner, K. Rissanen and J. R. Nitschke, White Phosphorus Is Air-Stable Within a Self-Assembled Tetrahedral Capsule, *Science*, 2009, **324**, 1697–1699.
17 Y.-H. Huang, Y.-L. Lu, J. Ruan, S.-P. Zheng, X.-D. Zhang, C.-H. Liu, Y.-H. Qin, Z.-M. Cao, Z. Jiao, H.-S. Xu and C.-Y. Su, Dynamic Metallosupramolecular Cages Containing 12 Adaptable Pockets for High-Order Guest Binding Beyond Biomimicry, *J. Am. Chem. Soc.*, 2023, **145**, 23361–23371.
18 L. S. Lisboa, D. Preston, C. J. McAdam, L. J. Wright, C. G. Hartinger and J. D. Crowley, Heterotrimetallic Double Cavity Cages: Syntheses and Selective Guest Binding, *Angew. Chem., Int. Ed.*, 2022, **61**, e202201700.
19 Y. Katagiri, Y. Tsuchida, Y. Matsuo and M. Yoshizawa, An Adamantane Capsule and its Efficient Uptake of Spherical Guests up to 3 nm in Water, *J. Am. Chem. Soc.*, 2021, **143**, 21492–21496.
20 F. J. Rizzuto, L. K. S. von Krbek and J. R. Nitschke, Strategies for binding multiple guests in metal-organic cages, *Nat. Rev. Chem.*, 2019, **3**, 204–222.
21 S. Hasegawa, S. L. Meichsner, J. J. Holstein, A. Baksi, M. Kasanmascheff and G. H. Clever, Long-Lived C_{60} Radical Anion Stabilized Inside an Electron-Deficient Coordination Cage, *J. Am. Chem. Soc.*, 2021, **143**, 9718–9723.
22 N. M. A. Speakman, A. W. Heard and J. R. Nitschke, A CuI_6L_4 Cage Dynamically Reconfigures to Form Suit[4]anes and Selectively Bind Fluorinated Steroids, *J. Am. Chem. Soc.*, 2024, **146**, 10234–10239.
23 W. Thor, A. N. Carneiro Neto, R. T. Moura Jr, K.-L. Wong and P. A. Tanner, Europium(III) coordination chemistry: structure, spectra and hypersensitivity, *Coord. Chem. Rev.*, 2024, **517**, 215927.
24 Z.-H. Pan, Z.-Z. Weng, X.-J. Kong, L.-S. Long and L.-S. Zheng, Lanthanide-containing clusters for catalytic water splitting and CO_2 conversion, *Coord. Chem. Rev.*, 2022, **457**, 214419.
25 F. Pointillart, M. Atzori and C. Train, Magneto-chiral dichroism of chiral lanthanide complexes, *Inorg. Chem. Front.*, 2024, **11**, 1313–1321.
26 N. Xu, W. Chen, Y.-S. Ding and Z. Zheng, A Cubic Tinkertoy-like Heterometallic Cluster with a Record Magnetocaloric Effect, *J. Am. Chem. Soc.*, 2024, **146**, 9506–9511.
27 Z. Zhu, S. Hu, Z. Liu, L. Zhou, C. Tian and Q. Sun, A cationic radical lanthanide organic tetrahedron with remarkable coordination enhanced radical stability, *Chin. Chem. Lett.*, 2025, **36**, 109641.
28 X.-Z. Li, C.-B. Tian and Q.-F. Sun, Coordination-Directed Self-Assembly of Functional Polynuclear Lanthanide Supramolecular Architectures, *Chem. Rev.*, 2022, **122**, 6374–6458.
29 D. J. Bell, L. S. Natrajan and I. A. Riddell, Design of lanthanide based metal-organic polyhedral cages for application in catalysis, sensing, separation and magnetism, *Coord. Chem. Rev.*, 2022, **472**, 214786.
30 D. L. Caulder and K. N. Raymond, Supermolecules by design, *Acc. Chem. Res.*, 1999, **32**, 975–982.
31 X.-Z. Li, L.-P. Zhou, L.-L. Yang, D.-Q. Yuan, C.-S. Lin and Q.-F. Sun, Evolution of Luminescent Supramolecular Lanthanide $M_{2n}L_{3n}$ Complexes from Helicates and Tetrahedra to Cubes, *J. Am. Chem. Soc.*, 2017, **139**, 8237–8244.

32 Z. Wang, L. He, B. Liu, L.-P. Zhou, L.-X. Cai, S.-J. Hu, X.-Z. Li, Z. Li, T. Chen, X. Li and Q.-F. Sun, Coordination-Assembled Water-Soluble Anionic Lanthanide Organic Polyhedra for Luminescent Labeling and Magnetic Resonance Imaging, *J. Am. Chem. Soc.*, 2020, **142**, 16409–16419.

33 X.-F. Duan, L.-P. Zhou, H.-R. Li, S.-J. Hu, W. Zheng, X. Xu, R. Zhang, X. Chen, X.-Q. Guo and Q.-F. Sun, Excited-Multimer Mediated Supramolecular Upconversion on Multicomponent Lanthanide-Organic Assemblies, *J. Am. Chem. Soc.*, 2023, **145**, 23121–23130.

34 X.-Z. Li, L.-P. Zhou, S.-J. Hu, L.-X. Cai, X.-Q. Guo, Z. Wang and Q.-F. Sun, Metal ion adaptive self-assembly of photo-active lanthanide-based supramolecular hosts, *Chem. Commun.*, 2020, **56**, 4416–4419.

35 Y. Liu, Z. Lin, C. He, L. Zhao and C. Duan, A symmetry-controlled and face-driven approach for the assembly of cerium-based molecular polyhedra, *Dalton Trans.*, 2010, **39**, 11122–11125.

36 L. Zhao, S. Qu, C. He, R. Zhang and C. Duan, Face-driven octanuclear cerium(IV) luminescence polyhedra: synthesis and luminescent sensing natural saccharides, *Chem. Commun.*, 2011, **47**, 9387–9389.

37 X. Tang, D. Chu, W. Gong, Y. Cui and Y. Liu, Metal-Organic Cages with Missing Linker Defects, *Angew. Chem., Int. Ed.*, 2021, **60**, 9099–9105.

38 Y. B. Tan, Y. Okayasu, S. Katao, Y. Nishikawa, F. Asanoma, M. Yamada, J. Yuasa and T. Kawai, Visible Circularly Polarized Luminescence of Octanuclear Circular Eu(III) Helicate, *J. Am. Chem. Soc.*, 2020, **142**, 17653–17661.

39 I. A. Riddell, Y. R. Hristova, J. K. Clegg, C. S. Wood, B. Breiner and J. R. Nitschke, Five Discrete Multinuclear Metal-Organic Assemblies from One Ligand: Deciphering the Effects of Different Templates, *J. Am. Chem. Soc.*, 2013, **135**, 2723–2733.

40 D. J. Bell, T. Zhang, N. Geue, C. J. Rogers, P. E. Barran, A. M. Bowen, L. S. Natrajan and I. A. Riddell, Hexanuclear Ln_6L_6 Complex Formation by Using an Unsymmetric Ligand, *Chem. – Eur. J.*, 2023, **29**, e202302497.

41 S.-J. Hu, X.-Q. Guo, L.-P. Zhou, L.-X. Cai, C.-B. Tian and Q.-F. Sun, Ionic Radius Dependent Kinetic Behavior for the Self-Assemblyand Chiral Amplification of Lanthanide Tetrahedral Cages, *Chin. J. Chem.*, 2023, **41**, 797–804.

42 Q. Bai, Y. Liu, T. Wu, H. Su, G. Chen, Y. Guan, M. Wang, T.-Z. Xie, Z. Zhang and P. Wang, Metal ion determined self-assembly using terpyridine building blocks, *Org. Chem. Front.*, 2022, **9**, 2343–2350.

43 Q.-F. Sun, S. Sato and M. Fujita, An $M_{18}L_{24}$ stellated cuboctahedron through post-stellation of an $M_{12}L_{24}$ core, *Nat. Chem.*, 2012, **4**, 330–333.

44 K. Endo, H. Ube and M. Shionoya, Multi-Stimuli-Responsive Interconversion between Bowl- and Capsule-Shaped Self-Assembled Zinc(II) Complexes, *J. Am. Chem. Soc.*, 2020, **142**, 407–416.

45 T.-Z. Xie, K. J. Endres, Z. Guo, J. M. Ludlow III, C. N. Moorefield, M. J. Saunders, C. Wesdemiotis and G. R. Newkome, Controlled Interconversion of Superposed-Bistriangle, Octahedron, and Cuboctahedron Cages Constructed Using a Single, Terpyridinyl-Based Polyligand and Zn^{2+}, *J. Am. Chem. Soc.*, 2016, **138**, 12344–12347.

46 J. A. Davies, T. K. Ronson and J. R. Nitschke, Twisted rectangular subunits self-assemble into a ferritin-like capsule, *Chem*, 2022, **8**, 1099–1106.

47 X.-Q. Guo, L.-P. Zhou, S.-J. Hu, L.-X. Cai, P.-M. Cheng and Q.-F. Sun, Hexameric Lanthanide-Organic Capsules with Tertiary Structure and Emergent Functions, *J. Am. Chem. Soc.*, 2021, **143**, 6202–6210.

48 R. Zhu, I. Regeni, J. J. Holstein, B. Dittrich, M. Simon, S. Prevost, M. Gradzielski and G. H. Clever, Catenation and Aggregation of Multi-Cavity Coordination Cages, *Angew. Chem., Int. Ed.*, 2018, **57**, 13652–13656.

49 S. M. Jansze and K. Seyerin, Palladium-Based Metal-Ligand Assemblies: The Contrasting Behavior upon Addition of Pyridine or Acid, *J. Am. Chem. Soc.*, 2019, **141**, 815–819.

50 L.-P. Zhou, X.-S. Feng, S.-J. Hu and Q.-F. Sun, Controlled Self-Assembly, Isomerism, and Guest Uptake/Release of Charge-Reversible Lanthanide-Organic Octahedral Cages, *J. Am. Chem. Soc.*, 2023, **145**, 17845–17855.

51 K.-H. Yim, C.-T. Yeung, H.-Y. Wong and G.-L. Law, Structural variation of self-assembled lanthanide supramolecular complexes induced by reaction conditions, *Inorg. Chem. Front.*, 2021, **8**, 2952–2964.

52 E. Benchimol, B.-N. T. Nguyen, T. K. Ronson and J. R. Nitschke, Transformation networks of metal-organic cages controlled by chemical stimuli, *Chem. Soc. Rev.*, 2022, **51**, 5101–5135.

53 A. M. Johnson, M. C. Young, X. Zhang, R. R. Julian and R. J. Hooley, Cooperative Thermodynamic Control of Selectivity in the Self-Assembly of Rare Earth Metal-Ligand Helices, *J. Am. Chem. Soc.*, 2013, **135**, 17723–17726.

54 M. Otte, P. F. Kuijpers, O. Troeppner, I. Ivanovic-Burmazovic, J. N. H. Reek and B. de Bruin, Encapsulation of Metalloporphyrins in a Self-Assembled Cubic M_8L_6 Cage: A New Molecular Flask for Cobalt-Porphyrin-Catalysed Radical-Type Reactions, *Chem. – Eur. J.*, 2013, **19**, 10170–10178.

55 W. Xue, T. K. Ronson, Z. Lu and J. R. Nitschke, Solvent Drives Switching between Λ and Δ Metal Center Stereochemistry of M_8L_6 Cubic Cages, *J. Am. Chem. Soc.*, 2022, **144**, 6136–6142.

56 W. Meng, B. Breiner, K. Rissanen, J. D. Thoburn, J. K. Clegg and J. R. Nitschke, A Self-Assembled M_8L_6 Cubic Cage that Selectively Encapsulates Large Aromatic Guests, *Angew. Chem., Int. Ed.*, 2011, **50**, 3479–3483.

57 W. Brenner, T. K. Ronson and J. R. Nitschke, Separation and Selective Formation of Fullerene Adducts within an MII_8L_6 Cage, *J. Am. Chem. Soc.*, 2017, **139**, 75–78.

58 V. Mouarrawis, E. O. Bobylev, B. de Bruin and J. N. H. Reek, A Novel M_8L_6 Cubic Cage That Binds Tetrapyridyl Porphyrins: Cage and Solvent Effects in Cobalt-Porphyrin-Catalyzed Cyclopropanation Reactions, *Chem. – Eur. J.*, 2021, **27**, 8390–8397.

59 L. Yang, X. Jing, C. He, Z. Chang and C. Duan, Redox-Active M_8L_6 Cubic Hosts with Tetraphenylethylene Faces Encapsulate Organic Dyes for Light-Driven H_2 Production, *Chem. – Eur. J.*, 2016, **22**, 18107–18114.

60 J. A. Davies, A. Tarzia, T. K. Ronson, F. Auras, K. E. Jelfs and J. R. Nitschke, Tetramine Aspect Ratio and Flexibility Determine Framework Symmetry for Zn_8L_6 Self-Assembled Structures, *Angew. Chem., Int. Ed.*, 2023, **62**, e202217987.

61 J. A. Davies, T. K. Ronson and J. R. Nitschke, Triamine and Tetramine Edge-Length Matching Drives Heteroleptic Triangular and Tetragonal Prism Assembly, *J. Am. Chem. Soc.*, 2024, **146**, 5215–5223.

62 L. J. K. Cook, R. Mohammed, G. Sherborne, T. D. Roberts, S. Alvarez and M. A. Halcrow, Spin state behavior of iron (II)/dipyrazolylpyridine complexes. New insights from crystallographic and solution measurements, *Coord. Chem. Rev.*, 2015, **289**, 2–12.

63 F. Yin, J. Yang, L.-P. Zhou, X. Meng, C.-B. Tian and Q.-F. Sun, 54 K Spin Transition Temperature Shift in a Fe_6L_4 Octahedral Cage Induced by Optimal Fitted Multiple Guests, *J. Am. Chem. Soc.*, 2024, **146**, 7811–7821.

64 M. Feng, F. Pointillart, B. Le Guennic, B. Lefeuvre, S. Golhen, O. Cador, O. Maury and L. Ouahab, Unprecedented Sensitization of Visible and Near-Infrared Lanthanide Luminescence by Using a Tetrathiafulvalene-Based Chromophore, *Chem. – Asian J.*, 2014, **9**, 2814–2825.

65 J. M. Stanley, X. Zhu, X. Yang and B. J. Holliday, Europium Complexes of a Novel Ethylenedioxythiophene-Derivatized Bis (pyrazolyl)pyridine Ligand Exhibiting Efficient Lanthanide Sensitization, *Inorg. Chem.*, 2010, **49**, 2035–2037.

66 X. Hu, W. Dou, C. Xu, X. Tang, J. Zheng and W. Liu, Lanthanide radii controlled one-dimensional polymer and dinuclear complexes and their fluorescent properties, *Dalton Trans.*, 2011, **40**, 3412–3418.

67 G. Li, X. Zhao, Q. Han, L. Wang and W. Liu, Radii-dependent self-assembly of chiral lanthanide complexes: synthesis, chirality, and single-molecule magnet behavior, *Dalton Trans.*, 2020, **49**, 10120–10126.

68 A. Vuillamy, S. Zebret, C. Besnard, V. Placide, S. Petoud and J. Hamacek, Functionalized Triptycene-Derived Tripodal Ligands: Privileged Formation of Tetranuclear Cage Assemblies with Larger Ln(III), *Inorg. Chem.*, 2017, **56**, 2742–2749.

69 H.-Y. Wong, W. T. K. Chan and G.-L. Law, Assembly of Lanthanide(III) Cubanes and Dimers with Single-Molecule Magnetism and Photoluminescence, *Inorg. Chem.*, 2018, **57**, 6893–6902.

70 D. Chakraborty, N. Kaur, J. Sahoo, N. Hickey, M. De and P. S. Mukherjee, Host-Guest Interactions Induced Enhancement in Oxidase-Like Activity of a Benzothiadiazole Dye Inside an Aqueous Pd_8L_4 Barrel, *J. Am. Chem. Soc.*, 2024, **146**, 24901–24910.

71 P. Howlader, B. Mondal, P. C. Purba, E. Zangrando and P. S. Mukherjee, Self-Assembled Pd(II) Barrels as Containers for Transient Merocyanine Form and Reverse Thermochromism of Spiropyran, *J. Am. Chem. Soc.*, 2018, **140**, 7952–7960.

72 J. B. Maglic and R. Lavendomme, MoloVol: an easy-to-use program for analyzing cavities, volumes and surface areas of chemical structures, *J. Appl. Crystallogr.*, 2022, **55**, 1033–1044.

73 S.-Y. Wu, X.-Q. Guo, L.-P. Zhou and Q.-F. Sun, Fine-Tuned Visible and Near-Infrared Luminescence on Self-Assembled Lanthanide-Organic Tetrahedral Cages with Triazole-Based Chelates, *Inorg. Chem.*, 2019, **58**, 7091–7098.

